Molecular Dynamics Study of the Structure and Dynamics of Water in Cylindrical Pores

C. Hartnig, W. Witschel, and E. Spohr*

Department of Theoretical Chemistry, University of Ulm, Albert-Einstein-Allee 11, D-89069 Ulm, Germany

Received: September 15, 1997; In Final Form: December 1, 1997

The structure and dynamics of confined water in cylindrical pores have been investigated by molecular dynamics simulations. Both rigid (TIP4P) and flexible (BJH) models have been used. Pore radii between 4.2 and 20 Å have been studied; the pore walls are modeled either as a smooth (10−4) Lennard-Jones wall or as a structured wall consisting of (12−6) Lennard-Jones particles. Polar functional groups on the pore surface are modeled by arrays of point charges. We present results on density and orientational distribution functions and on the water mobility. We observe that water transport through nonpolar pores is fast and dominated by the surface layer, whereas transport in polar pores is slowed down relative to bulk liquid water and occurs preferentially through the center of the pore.

1. Introduction

Polymer membranes are important system components in various disciplines of modern chemistry. Sulfonated and carboxylated poly(tetrafluoroethylene) membranes are used in fuel cells both as solid state electrodes (NAFION, Flemion, and other bifunctional membranes; see, for example, refs 1, 2, and references therein) and as a means to separate electrochemical cells, thus facilitating the flow of ionic charge but preventing the transfer of chemical species that might inhibit electrochemical processes. Another class of polymer membranes is ion-selective. These membranes usually consist of narrow pores. The necessary narrow size distribution of these pores can be achieved by different procedures. The gel-template-leaching method, as one example, was recently introduced by Gankema et al.[3] Using this technique, it is possible to synthesize pores in a polymeric membrane with a well-defined pore diameter between 4 and 145 nm and a very narrow size distribution (with root-mean-square deviation about ±10−15% of the expected diameter).[3,4] Ion selectivity is achieved by choosing the pore diameter to be approximately equal to the Debye length of the charged particles in the examined solution. An alternative is the modification of pore surfaces, either by saponification of the ester groups of poly(methyl methacrylate) or by functionalization with sulfonic acid groups. Such modified pores, and inorganic materials such as porous ceramics, have been studied by different NMR techniques with the goal of determining pore size distributions, effective radii, and arrangement and mobility of the molecules inside (e.g., ref 5).

Another class of porous materials with polar functional groups are glasses such as Vycor and Rhyolite, the properties of which have received much attention by experimentalists recently, because of their use as biosensors, selective gas permeation membranes, and catalysts. Vycor glass can be produced with a variety of well-defined pore diameters down to, for example, 40−60 Å, depending on the production process. The pore surfaces are covered with hydroxyl groups. These materials have been studied by neutron diffraction[6,7] and NMR spectroscopy.[8]

* To whom correspondence should be addressed. E-mail: eckhard.spohr@chemie.uni-ulm.de.

The above-described classes of pores are substantially wider in diameter than the biological ion channels. Ion-carrier molecules such as Gramicidin A have been studied extensively by computer simulation using different techniques and models (see, for example, refs 9−18 and references therein). In these channels, the mass transport is characterized by a synchronous translation of all molecules along the pore axis, termed single-file movement.[19,20]

In an ongoing project, we attempt to use computer simulations to understand ion mobility and selectivity in narrow synthetic pores. Before addressing this complex problem, we decided to systematically explore the dynamic behavior of the pure solvent, in this case water, first. We focus on the dynamics within the pore and do not investigate the process of entering or leaving the pore. In the present paper we report simulations of model pores with radii typical for the membranes used in fuel cells, in ion-selective membranes, and in Vycor glass. We first discuss several different models, which have various degrees of realism. Then, the pore size dependence of particle density, orientational profiles, and water mobility is analyzed, treating smooth, corrugated, charged, and very narrow pores consecutively.

II. Models and Methods

All systems are simulated using the rigid TIP4P water model.[21] In addition, the flexible BJH water model[22] has been used to investigate very narrow pores. The simulated systems contain between 50 and 730 water molecules and are thus much larger than the model pores simulated previously by other groups.[23,24] Some key parameters are summarized in Table 1.

In our calculations, the pore axis always points along the z direction. The simplest pore model (model I) used is a smooth cylinder. The smooth surface is described by a (10−4) Lennard-Jones potential of the form

$$V(\rho) = \epsilon\left[\left(\frac{\sigma}{\rho - \rho_0}\right)^{10} - \left(\frac{\sigma}{\rho - \rho_0}\right)^{4}\right] \qquad (1)$$

where ρ_0 indicates the radius of the pore, $\rho = \sqrt{x^2+y^2}$ the distance between the particle and the pore axis, ϵ the strength of the interactions, and σ the size parameter for the wall−oxygen

S1089-5647(97)03018-6 CCC: $15.00
Published on Web 01/23/1998

TABLE 1: Overview of Simulations[a]

run	ρ_0/Å	N	ϵ^*	L/Å	E_{total}/E_{Bulk}	E_S/mJ m^{-2}	t/ps	
S-R1[b]	4.2	135	1.22	80.6	0.18	117.2	250	
S-R2	6.7	171	1.22	88.32	0.65	−3.3	200	
S-R3	9.4	240	1.22	50.0	0.70	−4.2	200	
S-R4	11.6	288	1.22	33.94	0.73	−4.9	160	
S-R5	15.0	729	1.22	46.0	0.76	−5.2	200	
S-R6	20.3	719	1.22	22.98	0.75	−5.2	170	
S-E1	11.6	288	0.12	33.94	0.72	0.08	180	
S-E2	11.6	288	1.22	33.94	0.73	−4.9	160	
S-E3	11.1	288	2.44	33.94	0.74	−13.3	500	
S-E4	10.9	288	7.29	33.94	0.79	−51.0	200	
C-DH	11.6	288		33.94	0.75	−16.8	100	$N_C = 366$
C-HH	11.6	288		33.94	0.74	−11.0	120	$N_C = 240$
C-LI	11.6	288		33.94	0.74	−10.8	120	$N_C = 240$
CH36	10.9	288	7.29	33.94	0.92	−17.7	150	$n_q = 36$
CH72	10.9	288	7.29	33.94	0.91	−13.7	150	$n_q = 72$

[a] ρ_0 is the radius of the pore, N the number of water molecules, ϵ^* the reduced interaction parameter at 298.15 K, L the length of the periodic simulation cell, and t the simulation time. The total energy is given relative to the simulation value of a bulk simulation using the same water model ($E_{Bulk} = -40.66$ kJ/mol). E_S is the water−pore interaction energy divided by the pore area $2\pi\rho_0 L$. n_q is the number of external charges on the pore surface (runs CH*nn*), and N_C the number of carbon atoms on the corrugated pore surface. The acronyms C-DH, C-HH, and C-LI refer to double-helical, half-helical, and linear-chain pores, respectively (see Figure 1). [b] Several additional simulations with $50 \le N < 135$ have been performed.

interactions. We have set $\sigma = 2.5$ Å in all simulations. In the center of the pore, where ρ equals zero, the forces derived from the (10−4) LJ potential are discontinous but small. We have multiplied the potential with a switching function,

$$f_{sw}(\rho) = 0.5 \tanh(3.0(\rho - 1.0)) + 0.5 \qquad (2)$$

(ρ in Å), which leads to only very minor changes and could have been safely neglected, except for the narrowest pore diameters.

Like in studies of pure Lennard-Jones fluids, we introduce a dimensionless energy parameter ϵ^* ($=\epsilon/kT$, where k is Boltzmann's constant and T the temperature (298.15 K in all cases)).

Two series of simulations of pure water have been performed with model I. In one series, the pore radius ρ_0 was varied between 4.2 and 20.3 Å, keeping $\epsilon^* = 1.22$ constant. In the second series, the parameter ϵ^* was varied between 0.12 and 7.29 at a constant radius $\rho_0 \approx 11$ Å. In each of these simulations, ρ_0 was slightly adjusted in order to obtain the homogeneous bulk value for the water density in the center of the pore (see Table 1 for more details).

Model II is an extension of model I that includes the effect of surface corrugation. The smooth Lennard-Jones wall is replaced by arrangements of Lennard-Jones particles, which mimic naturally occurring structures. The parameters for the particles are calculated by the Lorentz−Berthelot rules from the C−C interactions in graphite[25] and the O−O interactions in the TIP4P model for water, yielding values of $\epsilon^*_{CO} = 0.16$ and $\sigma_{CO} = 3.3$ Å. These values are similar to those used by Roux and Karplus in their simulation of the Gramicidin A channel.[12] The Lennard-Jones particles are arranged in simple structures that also occur in biological systems: a single double-helix with 5 turns, 10 carbon chains with one-half turn over the height of the pore (like in connexons appearing in the gap junctions in eucaryotic biological membranes[26]), and 15 linear chains parallel to the pore axis (like crown ethers arranged in columnar structures[27]) (see also Figure 1 and Table 1). The radius of the pores is 11.6 Å.

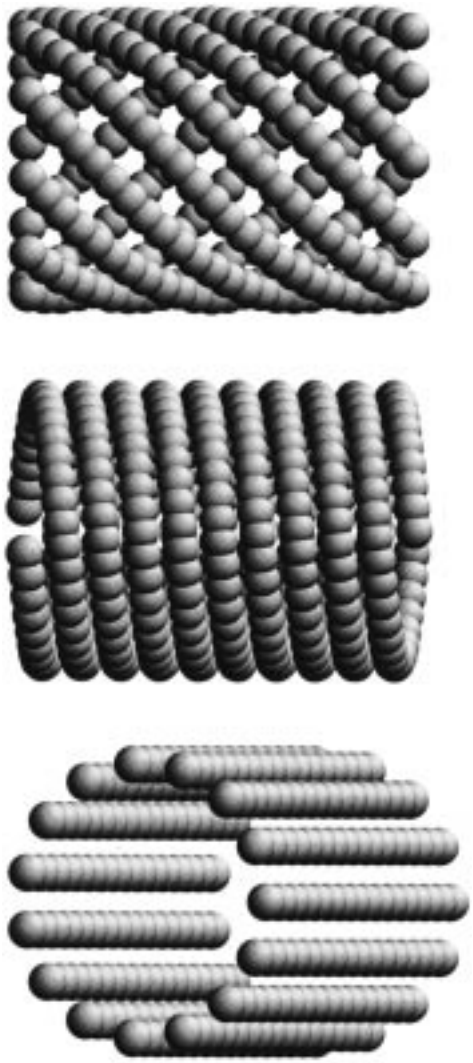

Figure 1. Arrangement of pore atoms for simulations of pores with atomic representation. Top: 10 half-helixes (run C-HH). Middle: 2 double-helixes (C-DH). Bottom: 15 linear chains (C-LI).

Model III is designed to investigate the electrical properties of pores in chemically modified membranes; it mimics polar functional groups on the pore wall. Unit elementary charges of alternating sign are arranged in helical form on the surface of a pore with $\rho_0 = 10.9$ Å and $\epsilon^* = 7.29$. $n_q = 36$ and 72 charges at $\rho_q = \rho_0 + 0.6$ Å form helices with 5 and 10 turns, respectively. The values and positions of the charges (q_j, x_j, y_j, z_j) are given by the formula

$$(q_j, x_j, y_j, z_j) = \left((-)^j e, \rho_q \cos\left(\frac{j\pi}{3.6}\right), \rho_q \sin\left(\frac{j\pi}{3.6}\right), -\frac{L}{2} + \frac{L}{n_q} j\right), \quad j = 0, \quad n_q - 1 \qquad (3)$$

e is the elementary charge and L is the length of the channel, which is periodically repeated along the z axis.

The equations of motion for the TIP4P model have been integrated by the SHAKE constraint algorithm with a time step length of 2.5 fs; those for the BJH model, by the Verlet algorithm with a time step length of 0.5 fs. The kinetic temperature was kept constant at 298.15 K by coupling to a Berendsen thermostat[28] with a time constant of 1.0 ps. The shifted-force method has been used to truncate all interaction at a cutoff radius $r_c = L/2$, where L is the length of the pore.

III. Results

Structural, energetic, and dynamical properties are investigated. Inhomogeneity and anisotropy in the pores are analyzed on the basis of density profiles and dipole moment profiles, respectively. Furthermore, the total energy of the system is compared to the total energy of bulk water at ambient conditions. Water dynamics is analyzed on the basis of the self-diffusion coefficient (SDC), which was calculated both from the mean square displacement (MSD) along the z direction via the Einstein relation

$$D = \lim_{t\to\infty} \frac{1}{2t} \langle [z_i(t) - z_i(0)]^2 \rangle \tag{4}$$

and from the autocorrelation function (ACF) c_{v_z} of the velocity component along the pore axis, v_z, according to[29]

$$D = \int_0^\infty c_{v_z}(t')\, dt' \tag{5}$$

In practice, the limit in eq 4 was replaced by fitting the slope of the MSD over the last third of the function, which was evaluated up to a total time of 25 ps. The upper limit in eq 5 has been chosen to be 2.5 ps. SDCs are calculated for several concentric cylindrical shells.

A. Smooth Pores. *1. Variation of Pore Radius ρ_0.* We have investigated pores over a wide range of radii, starting at very narrow pores ($\rho_0 = 4.2$) only slightly larger than Gramicidin A channels up to relatively wide pores of radius 20.3 Å, which is comparable in size to the smallest ones that have been realized by the gel-template-leaching method.[3] Table 1 summarizes the results of the runs. In cylindrical pores of diameters similar to the ones studied here, the number of molecules affected by the pore walls is substantially larger than in corresponding systems near flat interfaces. One indication is that the total energy of the system converges only very slowly to the bulk value. In the case of the nonfunctionalized pores, the reduction in the number of water−water interactions (due to the excluded volume) is obviously not balanced by the water−pore interactions. With the exception of the narrow pore with $\rho_0 = 4.2$ Å (see below), the water−pore interaction energy per unit pore area is roughly constant, indicating that the pressure is roughly the same in all cases.

The structure within the pores is best characterized on the basis of the atom density profiles. Figure 2 shows the oxygen density profiles along the laboratory ρ axis. In the narrow pores (up to $\rho_0 = 6.7$ Å), no homogeneous liquid water phase is formed. In the narrowest pore, a single off-axis density maximum is observed (see discussion below). Two maxima, one on-axis and one off-axis, are observed in the pore with $\rho_0 = 6.7$ Å. Starting at pore radii about 9 Å, a region of constant density forms in the center. The pore radius (or the number of molecules) is adjusted so that this region has the same density as bulk water at ambient conditions. It should be noted that this procedure, while easy to implement, does not lead to exactly the same chemical potential for all pores considered. The resulting density profiles are featureless for the larger pores and do not exhibit significant density oscillations because of the weak water−pore interactions. Similar to the case of water near smooth (9−3) LJ walls with a shallow minimum,[30] the densities decay monotonically to zero near the pore surface. As expected, the density along the pore axis is constant. An exception are the very narrow pores where, depending on the load in the pore, crystallization occurs (see below).

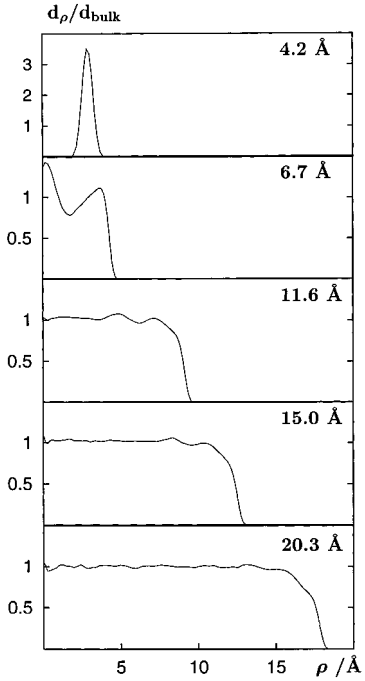

Figure 2. Oxygen density profiles for smooth pores of radius ρ_0 as indicated, normalized to the density of the bulk liquid.

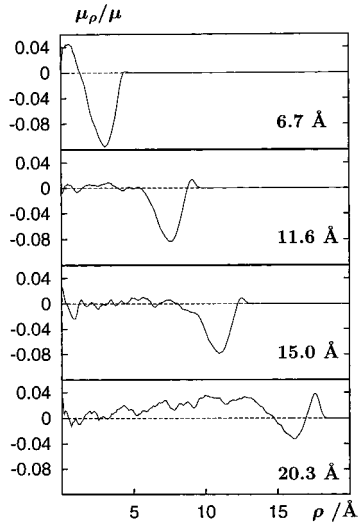

Figure 3. Average dipole moment (divided by the molecular dipole moment $\mu = 2.177$ D of the TIP4P model) as a function of the coordinate ρ in various smooth pores of radii as indicated.

We have further examined the orientational structure of water. Figure 3 shows the order parameter $\langle \mu_\rho/\mu \rangle(\rho)$, with μ_ρ the component of the dipole moment along the outward $\hat{\rho}$ direction perpendicular to the pore axis and μ the total dipole moment of the water model, respectively. Negative values indicate inward-pointing dipoles, i.e., molecules whose hydrogen atoms predominantly point to the pore axis. Values of -1 and 1 would indicate perfect antiparallel and parallel orientations, respectively. In the central part of the pore, where the density is constant, no preferences for specific dipole orientations are observed. Near the pore surface there is a trend for the hydrogen atoms to point into the polar aqueous phase. The minimum value of about -0.08 shows that the dipoles are far from being perfectly arranged. Only very near to the surface are there a few molecules in the low-density region with a tendency for the hydrogen atoms to point toward the pore surface. It should be noted that this orientational ordering is entirely due to the

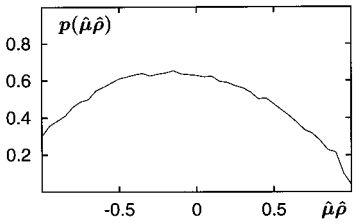

Figure 4. Distribution of the cosine of the angle between the outward $\hat{\rho}$ direction and the molecular dipole moment direction μ for water molecules in the range $\rho > 6$ in the pore with radius $\rho_0 = 11.6$ Å and $\epsilon^* = 1.22$.

TABLE 2: Self-Diffusion Coefficients (SDCs) in Pores with Smooth Surface Relative to the SDC of Pure Bulk Water ($D_{bulk} = 3.8 \times 10^{-5}$ cm^2 s^{-1})[a]

run	ρ_0/Å	region (Å)	r_1	r_2
S-R1	4.2	total	0.0	0.0
S-R2	6.7	0−2.2	1.7	1.6
		2.2−6.7	1.6	2.5
		total	1.6	2.3
S-R3	9.4	0−4.0	1.5	1.2
		4.0−9.4	1.5	2.1
		total	1.5	1.7
S-R4	11.6	0−4.0	1.4	1.0
		4.0−6.5	1.6	1.4
		6.5−11.6	1.7	1.7
		total	1.6	1.4
S-R5	15.0	0−5.0	1.0	1.0
		5.0−9.5	1.2	1.2
		9.5−15	1.4	1.7
		total	1.3	1.4
S-R6	20.3	0−6.0	1.1	1.1
		6.0−11.0	1.1	1.1
		11.0−14.0	1.3	1.2
		14.0−20.3	1.3	1.8
		total	1.2	1.4

[a] r_1 denotes the ratio of SDCs obtained up to a time $\tau_{corr} = 25$ ps; r_2, the corresponding ratio with $\tau_{corr} = 2.5$ ps. Data are given for different radial regions and for the total system. The relative standard deviation of the average, obtained by partitioning the simulation time into three or four equal intervals, is approximately 5%.

water−water interactions, since in model I the hydrogen atoms do not interact with the pore surface. Figure 4 shows, for the pore with $\rho_0 = 11.6$ Å, that the distribution of dipole orientations in the range $\rho > 6$ Å is rather broad, with orientations roughly perpendicular to the ρ directions being the most probable ones. This behavior is again similar to the one observed in simulations near planar interfaces. The corresponding data for the wider pores are very similar and, therefore, are not shown here. Orientational distributions along the z and ϕ directions should be isotropic due to the symmetry of the system. On the simulation time scales of between 150 and 250 ps we do observe nonvanishing total dipole moments along the pore axis. However, the fluctuations are small in magnitude and decrease with increasing simulation time, as the statistics improves.

Self-diffusion coefficients (SDCs) for the motion along the pore axis have been calculated according to eqs 4 and 5 for two different times, namely, 2.5 and 25 ps. The SDCs have been obtained separately for several concentric cylinder regions. Here, the molecule's assignment to a certain cylinder region is made on the basis of its position at zero time for the autocorrelation function; it is not changed when the molecule leaves the cylinder region during the correlation time. The results, relative to the SDC of pure bulk water using the same model and methods, are summarized in Table 2. For the shorter time, both the mean square displacements and the autocorrelation functions have been used and yield identical results within the limits of statistical uncertainty, while for the longer time only the mean square displacement was employed. The trends are similar in all systems: The SDC increases from the center toward the outer regions. The SDC is larger than in pure bulk water and approaches the pure water limit only very slowly with increasing pore radius. Hence, water transport is facilitated near the nonpolar pore surface, similar to the observed increases in simulated water near nonpolar planar interfaces.[31−34] In the cylindrical pores the overall enhancement of mobility is, because of the relatively larger surface area, larger than in the case of slit pores, as can be seen from the SDCs for total water.

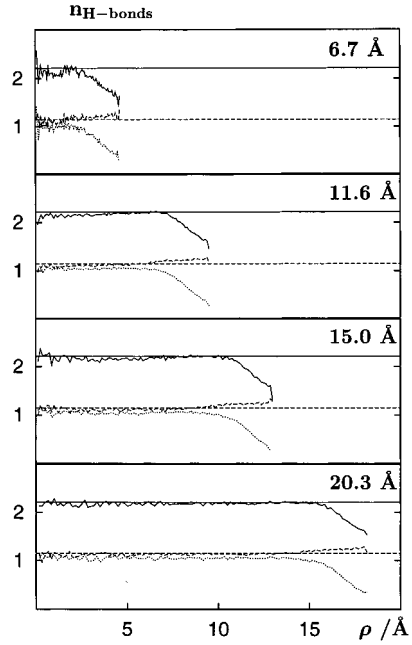

Figure 5. Number of hydrogen bonds per water molecule in pores with smooth surfaces and $\epsilon^* = 1.22$. Solid lines: total number of hydrogen bonds. Long dashed lines: donor bonds. Dotted lines: acceptor bonds (see text for definitions). The horizontal lines indicate the corresponding values in pure bulk TIP4P water for the total number (full line) and the number of donor hydrogen bonds (dashed), using the same definitions.

The ratios r_2, obtained from the correlation over 2.5 ps, show a larger variation between the inner and the outer pore regions than the corresponding ratios r_1, obtained from the correlation over 25 ps. The differences have their origin in the exchange of molecules between the various regions. The molecules near the pore surface, which initially diffuse relatively fast along the pore axis, move, within a few picoseconds, into the central region of the pores. Of course, once there, they acquire the smaller SDC characteristic of that region (but are still assigned for the purpose of the calculation to the surface region, vide supra). In the limit of infinite time, all subsets should exhibit the same diffusion coefficient. Hence, from the behavior of the SDCs it is clear that the exchange of molecules between the regions defined in Table 2 takes place on a time scale of several to several tens of picoseconds. This has also been verified by direct calculations of the residence autocorrelation functions (which yield residence times between 10 and 15 ps).

The increase in SDC is paralleled by a decrease of the number of hydrogen bonds near the pore surface, as is evident from Figure 5. Especially the number of "acceptor" hydrogen bonds, defined as those bonds in which the molecule under investigation interacts with the hydrogen atom of another molecule, decreases substantially close to the nonpolar pore surface. Simultaneously, the number of donor bonds, in which the hydrogen atom within

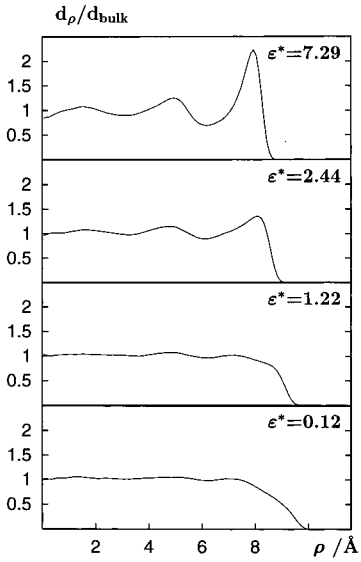

Figure 6. Oxygen density profiles for smooth pores with radius $\rho_0 \approx$ 11.6 Å and varying strength of adsorption, ϵ*, as indicated.

the molecule under investigation participates in the bond, increases slightly. The hydrogen atoms of the near-surface molecules thus point predominantly into the liquid, which is consistent with the average dipole moment in Figure 3. The net result, however, is a significant decrease in the total number of hydrogen bonds due to the geometric effect of the reduced coordination number. In other inhomogeneous systems[31−34] this effect is also known to increase water mobility.

2. Variation of ϵ*.* In a second series of simulations, the strength parameter ϵ* has been varied between the values 0.12 and 7.29. The values of ρ_0 are ∼11.6 Å and have been adjusted in order to achieve bulk water density in the center of the pores at a given particle number. Figure 6 shows the oxygen density profiles perpendicular to the pore axis. With increasing values of ϵ* the attractive forces between water and the pore surface become stronger and, for $\epsilon^* \geq 2.44$, an oscillatory density profile develops. For smaller values of ϵ* the density profile is monotonic and resembles that of the water/vacuum interface. Over the investigated range of the parameter ϵ* no significant changes in the orientational and hydrogen properties have been observed due to the fact that the changes in ϵ* do not affect the orientational interactions in a significant way.

Table 3 summarizes the mobility data for these pores. For all values of ϵ* the SDC is larger near the pore surface than in the center of the pore. However, with increasing ϵ*, the effect becomes smaller and at the highest value of ϵ* the SDC is almost homogeneous throughout the pore. The layering of the particles next to the pore surface obviously compensates the effect of the reduction of hydrogen bonds. The diffusion of a molecule parallel to the surface is hindered by the presence of other molecules directly in its path. This phenomenon is again similar to the behavior of water near planar interfaces where substantial layering due to strong adsorptive interactions reduces the diffusion coefficient parallel to the surface dramatically (see, for example, ref 35).

B. Narrow Pores. In pores with $\rho_0 < 5$ Å a dynamical behavior different from the larger pores is observed. Over periods of 1−2 ns the system changes from a liquidlike state with liquidlike mobility to one with vanishing SDC. We have investigated pores with $\rho_0 = 4.2$ Å and length $L = 80.6$ Å and occupancies between 50 and 135 water molecules. In all cases a tendency is observed to form rigid helical structures.

Figure 7 shows density profiles of oxygen and hydrogen

TABLE 3: Self-Diffusion Coefficients in Pores of Radius = 11.6 Å as a Function of the Strength of the Water−Pore Interaction, Characterized by the Parameter ϵ*, Relative to the SDC of Pure Bulk Water ($D_{bulk} = 3.8 \times 10^{-5}$ cm^2 s^{-1})[a]

run	ϵ*	region (Å)	r_1	r_2
S-E1	0.12	0−4.0	1.5	0.9
		4.0−6.5	1.7	1.3
		6.5−11.6	1.7	1.8
		total	1.6	1.5
S-E2	1.22	0−4.0	1.4	1.0
		4.0−6.5	1.6	1.4
		6.5−11.6	1.7	1.7
		total	1.6	1.4
S-E3	2.44	0−3.2	1.0	1.0
		3.2−6.0	1.2	1.1
		6.0−11.1	1.4	1.7
		total	1.3	1.4
S-E4	7.29	0−4.5	1.1	1.0
		4.5−7.0	1.1	1.0
		7.0−10.9	1.1	1.4
		total	1.1	1.2

[a] r_1 denotes the ratio of SDCs obtained up to a time $\tau_{corr} = 25$ ps; r_2, the corresponding ratio with $\tau_{corr} = 2.5$ ps. Data are given for different radial regions and for the total system. The relative standard deviation of the average, obtained by partitioning the simulation time into three or four equal intervals, is approximately 5%.

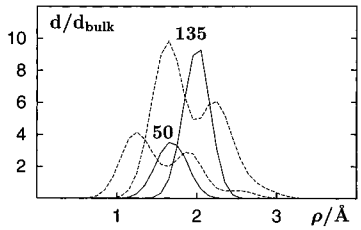

Figure 7. Radial density distributions of oxygen (full lines) and hydrogen atoms (dashed) in a pore with parameters $\rho_0 = 4.2$ Å and $\epsilon^* = 1.22$. Higher densities are for $N = 135$; lower densities are for $N = 50$ water molecules.

atoms for the lowest and highest simulated occupancy of the channel, taken over the final 500 ps. The molecules are preferentially located off the pore axis. With increasing occupancy of the channel, the molecules are pushed further into the soft pore wall. The energetic expense of the more repulsive water−pore interactions is apparently balanced by water−water interactions. The hydrogen atom distributions are bimodal. Most hydrogen atoms point to the center of the pore; the second maximum of the hydrogen density profile at slightly larger distances than the oxygen atom maxima corresponds to nonlinear hydrogen bonds along the pore axis.

Figure 8 shows final configurations after 2 ns of several runs at different channel occupancies. All simulations were started from disordered configurations similar to the one at the top of the figure for $N = 50$. Over the first several hundred picoseconds the SDC indicates fluidlike behavior. Then the helical structures develop while the total energy and the SDC decrease monotonically. At the end of the 2-ns simulation interval the SDC is equal to zero within the error limits. We did not follow these systems until convergence was achieved. One can expect that more (probably not all) of the defects vanish. In the near future we plan to investigate these narrow pores in more detail by coupling the channel to a bulk liquid phase.

C. Structured Pores. In a subsequent series of runs, we have investigated the role of the atomic structure of the surface on structural and dynamical properties, using model II of section II. Three different arrangements of atoms on the pore surface

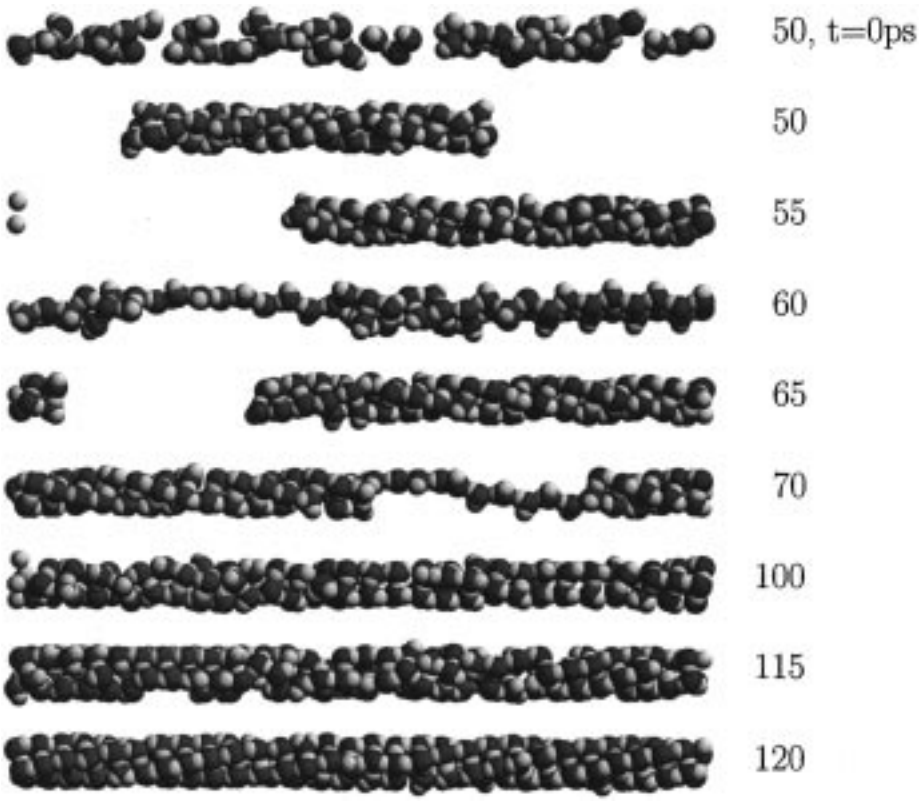

Figure 8. Snapshots of final configurations of water in a narrow pore ($\rho_0 = 4.2$ Å), at various channel occupancies as indicated. Also shown, as an example, is the initial configuration for the $N = 50$ run.

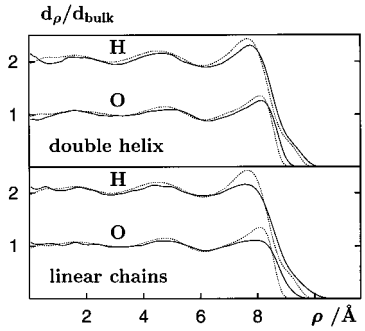

Figure 9. Oxygen and hydrogen atom density profiles in structured pores. Top: double helical structure (see Figure 1, middle). Bottom: linear chain structure (see Figure 1, bottom). The oxygen and hydrogen atom profiles are normalized to 1 and 2, respectively. The density profiles of the smooth pore with $\epsilon^* = 2.44$ are given for comparison (dotted lines).

were investigated for pores with radius $\rho_0 = 11.6$ Å, as depicted in Figure 1. Table 1 indicates that the total energy is similar to the smooth pore with $\epsilon^* = 2.44$. The water−pore interaction energy is more attractive than for run S-E3 in the double-helical pore and less attractive in the half-helical and linear-chain pores. The difference is due to the different numbers of atoms on the pore surface, 366 and 240 for simulation C-DH and for simulations C-HH and C-LI, respectively. Indeed, the density profiles for the double-helical pore depicted in the top frame of Figure 9 are very similar to the smooth pore. In the linear-chain pore (bottom frame of Figure 9) the oscillations of the density profiles are less pronounced. The half-helix pore is not shown here since the results are almost identical to those of the linear-chain pore. Also, the average dipole orientation along the ρ axis is similar to that in the pore S-E3. In keeping with the similar structure, the results in Table 4 indicate dynamics in the structured pores similar to those in simulation S-E3. The

TABLE 4: Self-Diffusion Coefficients in Systems with Structured Pores; Values Are Given Relative to the SDC of Pure Bulk Water ($D_{bulk} = 3.8 \times 10^{-5}$ cm^2 s^{-1})[a]

simulation	region (Å)	r_1	r_2
C-DH	0−4.0	1.2	1.0
	4.0−6.5	1.3	1.2
	6.5−11.6	1.3	1.7
	total	1.3	1.4
C-HH	0−4.0	1.2	0.9
	4.0−6.5	1.5	1.3
	6.5−11.6	1.5	1.8
	total	1.4	1.4
C-LI	0−4.0	1.2	0.9
	4.0−6.5	1.3	1.2
	6.5−11.6	1.6	1.8
	total	1.4	1.4

[a] r_1 denotes the ratio of SDCs obtained up to a time $\tau_{corr} = 25$ ps; r_2, the corresponding ratio with $\tau_{corr} = 2.5$ ps. Data are given for different radial regions and for the total system. The relative standard deviation of the average, obtained by partitioning the simulation time into three or four equal intervals, is approximately 5%.

SDCs in the two pores with weaker water−pore interactions (C-HH and C-LI) are higher than in the C-DH pore.

D. Charged Pores. The influence of surface polarity on the properties of water-filled pores was studied in two simulations of smooth pores with 36 (run CH36) or 72 (CH72) alternating positive and negative elementary charges on the pore surface (model III in section II; see also Table 1). The presence of the surface charges changes the energetics of the pore; the total energy of the system is significantly more negative than that of water in nonpolar pores. Figure 10 compares the oxygen and hydrogen atom density in the charged pore CH72 with the corresponding density profiles of the pore S-E4 without surface charges. In both runs the density profiles of oxygen and hydrogen atoms are similar and oscillatory. The density maxima near the pore surface are shifted to larger ρ values due to the

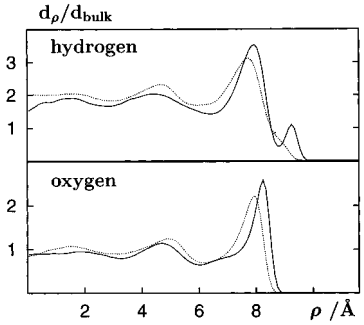

Figure 10. Oxygen and hydrogen density distribution for simulation CH72 with 72 charges on the pore wall. The dotted lines indicate the corresponding density distributions of the nonpolar system S-E4.

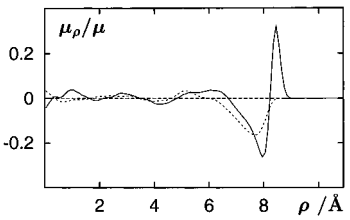

Figure 11. Average dipole moment (divided by the molecular dipole moment $\mu = 2.177$ D of the TIP4P model) as a function of the coordinate ρ in the pore CH72 with 72 alternating charges on the pore wall. The dotted lines indicate the corresponding function in the nonpolar system S-E4.

TABLE 5: Self-Diffusion Coefficients in Systems with Charged Pores; Values Are Given Relative to the SDC of Pure Bulk Water ($D_{bulk} = 3.8 \times 10^{-5}$ cm^2 s^{-1})[a]

simulation	region (Å)	r_1	r_2
CH36	0−3.0	0.7	0.9
	3.0−6.0	0.7	0.9
	6.0−10.9	0.6	0.7
	total	0.7	0.8
CH72	0−3.0	0.8	0.9
	3.0−6.0	0.7	0.8
	6.0−10.9	0.4	0.4
	total	0.6	0.6

[a] r_1 denotes the ratio of SDCs obtained up to a time $\tau_{corr} = 25$ ps; r_2, the corresponding ratio with $\tau_{corr} = 2.5$ ps. Data are given for different radial regions and for the total system. The relative standard deviation of the average, obtained by partitioning the simulation time into three or four equal intervals, is approximately 5%.

attraction by the surface charges. In the hydrogen atom density profile a small maximum around $\rho = 9.2$ Å develops. This feature is a consequence of the attraction of hydrogen atoms by the negative surface charges, which is not balanced by a short-range Lennard-Jones repulsion as in the case of oxygen (see section II). The average dipole moment along the ρ axis is shown in Figure 11 for runs CH72 and S-E4. Like in the nonpolar pore, there is a predominance in the range 6.7 Å < ρ < 8.2 Å for the water dipoles to point toward the center of the pore. In the polar pore, there is an additional region $\rho >$ 8.2 Å, where the dipoles point toward the pore surface, consistent with the hump in the hydrogen density profile at $\rho = 9.2$ Å. The change in dipole orientation across the first layer is reminiscent of double-layer structures in the case of planar interfaces between water and metallic surfaces.[35−40]

Table 5 documents a substantial influence of the surface charges on the water dynamics. Contrary to the nonpolar pores, the SDC is smaller than in bulk water. Furthermore, the SDC decreases from the center of pores toward the pore surface, while it increases in the same direction in nonpolar pores. It also decreases with the number of surface charges, which reflects the increasing immobilization of water molecules caused by the interaction of molecules with the surface charges, similar to the immobilization in the hydration shell of cations and anions (ref 39 and references therein). The fact that the pair correlation functions between surface charges and oxygen and hydrogen atoms (not shown) exhibit similar features as the corresponding ion−water radial distribution functions in a NaCl solution supports this view.

IV. Summary and Discussion

We have simulated confined water in cylindrical pores with diameters ranging from 8 to 42 Å using models of atomically smooth as well as corrugated pore surfaces, and of smooth pores with embedded point charges, to model functionalized pores. The study is part of a larger program to understand ion mobility in synthetic membrane pores. The purpose of the present work is to obtain an overview of the properties of pure water in various simple models of cylindrical pores. To that end, static and dynamic properties of water are analyzed on the basis of radial density distributions, radial polarization profiles, hydrogen bond statistics, and self-diffusion coefficients (SDCs). Some general trends emerge, which will be summarized below.

In nonpolar pores, the density oscillations increase with the water−pore interaction energy. At the same time, corrugation (introduced by modeling the pore surface through several different arrays of nonpolar centers) does not change the radial density profiles very much, provided that the interaction energies are similar (compare, for example, the properties of simulations C-DH, C-LI, and C-E3 in Table 1 and Figure 9). Modification of the pore with polar groups (modeled by arrays of alternating positive and negative charges on the pore surface) does not change the oxygen atom density profiles much (see Figure 10). An additional maximum of the hydrogen atom density profile characterizes the hydration of the negative surface charges by hydrogen bonds. Since in our models the hydrogen atoms are unaffected by the repulsive part of the water−pore interaction, they are able to move close to the negative charges on the pore walls, in a manner analogous to the hydration of negative ions.[39]

The orientational structure of water near nonpolar pore surfaces is dominated by the same principles as the orientational structure of water near planar surfaces. For water near two-dimensional surfaces it was convincingly shown that the compromise between the geometrical constraint and the optimization of the hydrogen bond network gives rise to the observed structures with molecular dipoles in the contact layer preferentially parallel to the surface. The orientational anisotropy is confined mostly to the first layer.[34,41] In the present work, the center of the pores is more or less isotropic. The dipoles of molecules in the first layer, which are in contact with the pore surface, show a slight preference for pointing into the liquid phase (Figure 3). The corresponding distribution functions (see Figure 4 as an example) are broad and indicate a preference for orientations in which the dipole moment is perpendicular to the $\hat{\rho}$ axis and thus parallel to the pore surface. The anisotropy of the distribution function gives rise to the observed small dipole moments in the first layer. Since the pore surface is strongly curved, hydrogen bonds between two water molecules more or less flat on the pore surface will usually lead to a dipole moment component along the $-\hat{\rho}$ direction. This dipole moment component becomes indeed smaller with decreasing curvature (or increasing radius ρ_0, see Figure 3), approaching the limiting value of the planar surface where the dipole moment perpendicular to the surface is very small. In polar modified pores, the hydration of negative surface charges

changes only the preferential orientation of molecules very close to the surface (see Figure 11).

The introduction of surface charges leads to substantial changes in the transport properties and reorientational dynamics of a pore. In all nonpolar pores, the self-diffusion coefficient (SDC) along the pore axis of molecules close to the surface is larger than the SDC of molecules in the center of the pore. The increased diffusion coefficient is a consequence of the reduced number of hydrogen bonds near the pore surface (see Figure 5). In all investigated cases with pore diameters between 13 and 40 Å the total diffusion coefficient along the pore axis is increased substantially relative to bulk liquid water; dipolar relaxation times (not shown) are also shorter than in the bulk liquid. On the other hand, the SDC in the polar pores decreases with increasing proximity of the water molecule to the pore surface. The total diffusion coefficient is reduced in comparison with the bulk liquid, and dipolar relaxation times are larger than in the bulk. Contrary to our results, Sansom et al.[23] observed, in nonpolar pores, an overall reduction of mobility for all pores with diameter less than 24 Å. One difference between the present work and ref 23 is that we calculate the self-diffusion coefficient only in the direction along the pore axis, since the mean square displacement perpendicular to the pore axis must approach a constant value in the infinite time limit and thus cannot contribute to the transport coefficient, while they use the total SDC in the short time limit. Another possible reason for the discrepancy might be small differences in pore occupancy and the differences in water−pore interactions. These differences can be assessed by performing simulations under chemical potential control, which are currently under way in our group.

Water in Vycor glass of pore sizes on the order of 40 to 60 Å in diameter exhibits similar structural features as bulk water in elastic neutron scattering.[6] With decreasing filling the local self-diffusion coefficient (describing the mobility within the pores) from inelastic neutron scattering decreases, indicating strong immobilization of the water fraction adsorbed on the surface.[7] Kimmich and co-workers[5] also observe slightly reduced diffusion coefficients in various ceramics and glasses. On the other hand, in porous silica glasses containing larger pores on the order of 500−2000 Å in diameter,[42] the NMR self-diffusion coefficient of water increases with decreasing filling. The fact that our simulations are consistent with the inelastic neutron scattering experiments on Vycor pores of similar diameter gives some confidence that the predictions of our model are qualitatively correct for the nonpolar pores, for which no direct experimental evidence is available. Furthermore, the increase of the diffusion of the polar molecule water due to the absence of wetting on the nonpolar surface seems to be analogous to the experimentally observed increase of the diffusion of the nonpolar molecule toluene in polar Vycor pores.[43]

Very narrow pores with diameters less than about 10 Å show very interesting nonequilibrium properties over times of 2 ns. Water forms solidlike, helical structures, in which the self-diffusion coefficient is reduced by several orders of magnitude. The investigation of this phenomenon, whether it is a physical effect or due to the simulation conditions, is the subject of an ongoing study. Sansom et al.[23] did not find a comparable drastic reduction of mobility in very narrow pores. However, the typical simulation time in their study was only on the order of 40 ps, too short, as our experience shows, to obtain a reliable long-term value of the SDC. Lynden-Bell and Rasaiah[24] observed a drastic reduction of mobility only in pores with a single-file arrangement of water molecules. Their simulations lasted for 5 ns but contained only very few molecules.

In summary, water-filled narrow pores show interesting dynamic properties. Water transport through nonpolar pores is fast and dominated by the surface layers of water, while the transport in polar pores is slow and occurs mainly through the center of the pore. We are currently investigating the consequences of this behavior on conductivity and selectivity of ion transport in electrolyte solutions.

Acknowledgment. Financial support by the Clothilde-Eberhardt-Foundation and Fonds der Chemischen Industrie and generous grants of computer time at the Computer Center of the University of Karlsruhe are gratefully acknowledged.

References and Notes

(1) Gierke, T. D.; Munn, G. E.; Wilson, F. C. *J. Polym. Sci. Pol. Phys.* **1981**, *19*, 1687.

(2) Eisenberg, A.; Yeager, H. L. *Perfluorinated Ionomer Membranes*; ACS Symposium Series 180; American Chemical Society: Washington, DC, 1982.

(3) Gankema, H.; Hempenius, M. A.; Möller, M. *Recl. Trav. Chim. Pay-Bas* **1994**, *113*, 241.

(4) Beginn, U. Personal communication.

(5) Kimmich, R.; Stapf, S.; Callaghan, P.; Coy, A. *Magn. Reson. Imag.* **1994**, *12*, 339.

(6) Bellissent-Funel, M. C.; Lal, J.; Bosio, L. *J. Chem. Phys.* **1993**, *98*, 4246.

(7) Bellissent-Funel, M. C.; Chen, S. H.; Zanotti, J. M. *Phys. Rev. E* **1995**, *51*, 4558.

(8) Bellissent-Funel, M. C.; Bradley, K. F.; Chen, H.; Lal, J.; Teixeira, J. *Physica A* **1993**, *201*, 277.

(9) Roux, B.; Karplus, M. *Annu. Rev. Biophys. Biomol. Struct.* **1994**, *23*, 731.

(10) Poxleitner, M.; Seitz-Beywl, J.; Heinzinger, K. *Z. Naturforsch.* **1993**, *48c*, 654.

(11) Andersen, O. S. *Annu. Rev. Physiol.* **1984**, *46*, 531.

(12) Roux, B.; Karplus, M. *Biophys. J.* **1991**, *59*, 961.

(13) Roux, B.; Karplus, M. *J. Phys. Chem.* **1991**, *95*, 4856.

(14) Roux, B.; Karplus, M. *J. Am. Chem. Soc.* **1993**, *115*, 3250.

(15) Kim, K.; Nguyen, H.; Swaminathan, P.; Clementi, E. *J. Phys. Chem.* **1985**, *89*, 2870.

(16) Finkelstein, A.; Andersen, O. S. *J. Membr. Biol.* **1981**, *59*, 155.

(17) Schlenkrich, M.; Bopp, P.; Skerra, A.; Brickmann, J. Structure and Dynamics Of Water On Membrane Surfaces and In Narrow Transmembrane Channels−Molecular Dynamics Simulations. In *Through Membranes: Carriers, Channels and Pumps. Proceedings of the 21st Jerusalem Symposium on Quantum Chemistry and Biochemistry*; Pullman, A., Jortner, J., Pullman, B., Eds.; Kluwer Academic Publishers: Israel, Dordrecht, 1988; pp 219−235.

(18) Breed, J.; Kerr, I. D.; Sankararamakrishnan, R.; Sansom, M. S. P. *Biophys. J.* **1996**, *70*, 1643.

(19) Hahn, K.; Kaerger, J. *J. Phys. A: Math. Gen.* **1995**, *28*, 3061.

(20) Hahn, K.; Kaerger, J. *J. Chem. Phys.* **1996**, *100*, 316.

(21) Jorgensen, W.; Chandrasekhar, J.; Madura, J. *J. Chem. Phys.* **1983**, *79*, 926.

(22) Bopp, P.; Jancsó, G.; Heinzinger, K. *Chem. Phys. Lett.* **1983**, *98*, 129.

(23) Sansom, M. S. P.; Kerr, I. D.; Breed, J.; Sankararamakrishnan, R. *Biophys. J.* **1996**, *70*, 693. See ref 24.

(24) Lynden-Bell, R. M.; Rasaiah, J. C. *J. Chem. Phys.* **1996**, *105*, 9266.

(25) Rhykerd, C.; Tan, Z.; Pozhar, L.; Gubbins, K. E. *J. Chem. Soc., Faraday Trans.* **1991**, *87*, 2011.

(26) Stryer, L. *Biochemistry*; W. H. Freeman and Co.: New York, 1988.

(27) Percec, V.; Heck, J.; Lee, M.; Ungar, G.; Alvarez-Castillo, A. *J. Mater. Chem.* **1992**, *2*, 1033.

(28) Berendsen, H. J. C.; Postman, J. P. M.; van Gunsteren, W. F.; DiNola, A.; Haak, J. R. *J. Chem. Phys.* **1984**, *81*, 3684.

(29) Allen, M. Tildesley, D. *Computer Simulation of Liquids*; Clarendon Press: Oxford, 1987; Chapter 2.7.

(30) Spohr, E. *J. Chem. Phys.* **1997**, *106*, 388.

(31) Sonnenschein, R.; Heinzinger, K. *Chem. Phys. Lett.* **1983**, *102*, 550.

(32) Spohr, E.; Heinzinger, K. *J. Chem. Phys.* **1986**, *84*, 2304.

(33) Wallqvist, A. *Chem. Phys. Lett.* **1990**, *165*, 437.

(34) Lee, S. H.; Rossky, P. J. *J. Chem. Phys.* **1994**, *100*, 3334.

(35) Spohr, E. *Chem. Phys.* **1990**, *141*, 87.
(36) Nagy, G.; Heinzinger, K. *J. Electroanal. Chem.* **1990**, *296*, 549.
(37) Nagy, G.; Heinzinger, K.; Spohr, E. *Faraday Discuss.* **1992**, *94*, 307.
(38) Heinzinger, K. *Pure Appl. Chem.* **1991**, *63*, 1733.
(39) Heinzinger, K. In *Computer Modelling Of Fluids Polymers and Solids*; Catlow, C. R. A., et al., Eds.; Kluwer Academic Publishers: Dordrecht, 1990; Chapter: Molecular Dynamics Simulations of Aqueous Systems, pp 357−394.
(40) Heinzinger, K. In *Structure of Electrified Interfaces, Frontiers of Electrochemistry*; Lipkowski, J., Ross, P. N., Eds.; VCH: New York, 1993; Chapter 7: Molecular Dynamics of Water at Interfaces, p 239.
(41) Spohr, E. *J. Phys. Chem.* **1989**, *93*, 6171.
(42) D'Orazio, F.; Bhattacharja, S.; Halperin, W. P. *Phys. Rev. Lett.* **1989**, *63*, 43.
(43) Abeles, B.; Chen, L. F.; Johnson, J. W.; Drake, J. M. *Isr. J. Chem.* **1991**, *31*, 99.